Nanoscale

Accepted Manuscript

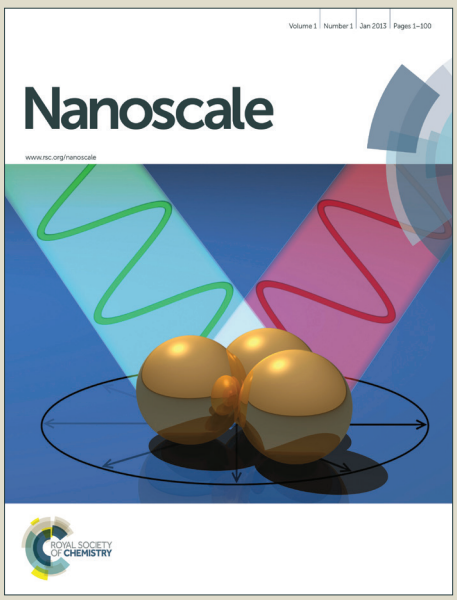

ROYAL SOCIETY OF CHEMISTRY

www.rsc.org/nanoscale

Nanoscale

ARTICLE

Ultrafast Colorimetric Determination of Predominant Protein Structure Evolution with Gold Nanoplasmonic Particles

Received 00th January 20xx,
Accepted 00th January 20xx

DOI: 10.1039/x0xx00000x

www.rsc.org/

Hye Young Kim and Inhee Choi*

The intracellular and extracellular accumulation of disordered proteins and aggregated proteins occurs in many protein conformational diseases, such as aging-related neurodegeneration and alcoholic liver diseases. However, the conventional methods to study protein structural changes are limited for the rapid detection and monitoring of protein aggregation because of long incubation times (i.e., usually several days), complicated sample pretreatment steps, and expensive instrumentation. Here, we describe an ultrafast colorimetric method for the real-time monitoring of protein structure evolution and the determination of predominant structures via nanoparticle-assisted protein aggregation. During the aggregation process, nanoparticles act as nucleation cores, which form networks depending on the structures of the protein aggregates, and accelerate the kinetics of the protein aggregation. Simultaneously, these nanoparticles exhibit colorimetric responses according to their embedded shapes (e.g., fibrillar and amorphous) on the protein aggregates. We observed distinct spectral shifts and concomitant colorimetric responses of concentration- and type-dependent protein aggregation with the naked eye within a few minutes (< 2 min) under acidic conditions. Moreover, the morphological transition from small aggregates to larger aggregates of nanoparticle-assisted protein aggregates were visualized with dark-field microscope imaging, which show a similar trend with that of protein aggregates formed without the aid of nanoparticles. Finally we show that our proposed method can be utilized to screen the protein aggregation propensity under a variety of conditions such as different pH levels, high temperature, and chemicals. These findings suggest that the proposed method is an easy way to study the molecular biophysics of protein aggregation and to rapidly screen anti-aggregation drugs for protein conformational diseases.

Introduction

Unfolded or misfolded proteins undergo conformational rearrangements that can induce undesired protein aggregation, and these proteins can become deposited within tissues or cellular compartments.[1, 2] The continuous deposition of abnormal proteins results in the onset of protein conformational diseases, including neurodegenerative diseases and alcoholic liver disease.[1, 3] Therefore, a thorough understanding of the kinetics and mechanisms of the formation and accumulation of protein aggregates is very important in elucidating the pathogenesis of protein conformational diseases. Recently, many researchers have made efforts to determine specific protein structural properties through the use of various methods, such as circular dichroism (CD) spectroscopy,[4] nuclear magnetic resonance spectroscopy,[5, 6] fluorescence spectroscopy,[7] and X-ray crystallography.[8] These methodologies can precisely detect the structural characteristics of proteins. However, their long incubations, complex pretreatment steps, and high cost hinder the rapid detection and monitoring of protein aggregation. Because of these limitations, the development of a faster, simpler, and easier method would be beneficial in protein aggregation research.

Recently, nanoscale plasmonic particles have received a lot of attention due to their tunability, biocompatibility, photostability, and excellent optical properties acting as Raman signal enhancers,[9-11] circular dichroism activators,[12, 13] and colorimetric reporters.[14-19] Assemblies of these nanoparticles[10, 13, 20, 21] are usually utilized for enhancing optical signals. Specifically, nanoparticles assembled with proteins can act as colorimetric reporters for studying protein structure evolution based on the distance-dependent light scattering of nanoparticles with the naked eye.[14-17] Chah et al. have shown that gold nanoparticles can be utilized as a colorimetric sensor for detecting dynamic conformational changes of redox active cytochrome *c*.[14] Hong et al. reported that protein monomer-conjugated gold nanoparticles can detect their own protein aggregates.[15] We previously described another approach demonstrating that protein aggregation under protein-destabilizing conditions (i.e., metal ions and acids) can be detected by the self-association of nanoparticles in the protein structural backbone as protein aggregation progresses.[16, 17] In a recent report, the catalytic role of nanoparticles that permits the rapid colorimetric detection of protein aggregation suggested that nanoparticles

Department of Life Science, University of Seoul, 163 Siripdae-ro, Dongdaemun-gu, Seoul 130-743, Republic of Korea. E-mail: inheechoi1@uos.ac.kr
†Electronic Supplementary Information (ESI) available. See DOI: 10.1039/x0xx00000x

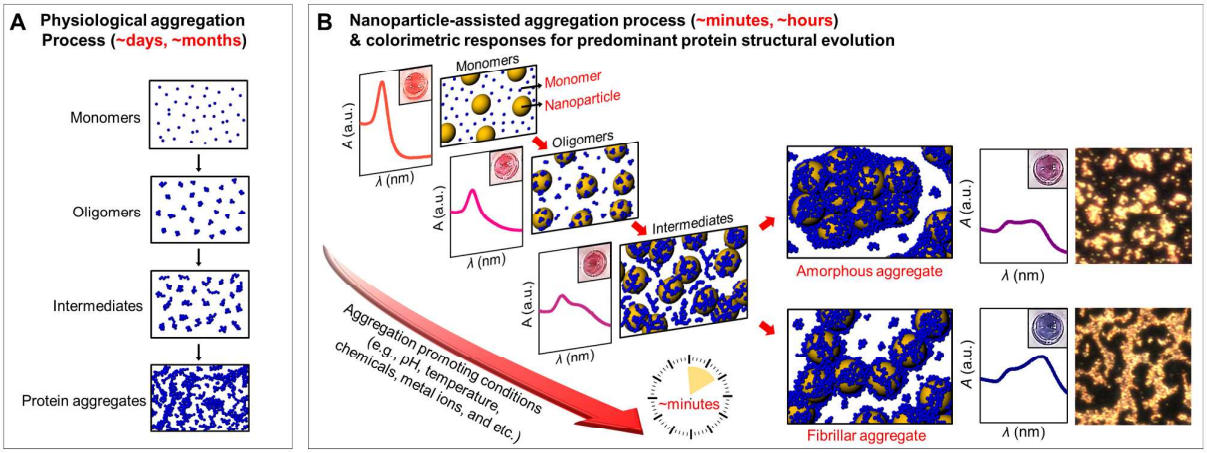

Scheme 1. Schematic illustrations of the nanoparticle-assisted protein structure evolution and its concomitant color transition. (A) Cartoon of the physiological aggregation process involving monomers, oligomers, intermediates, and large protein aggregates. (B) Illustration of the nanoparticle-assisted aggregation process, concomitant spectral and colorimetric responses, and representative morphologies of the aggregates.

could be used as nucleation cores for further protein aggregation.[17] Based on these findings, we hypothesized that we could quickly predict the propensity of protein aggregation and the predominant protein structures under certain destabilizing conditions by using nanoparticles as nucleation cores.

In this study, we suggest the use of an ultrafast colorimetric method for determining predominant protein structure evolution through nanoparticle-assisted protein aggregation. The approach we used to study protein aggregation is illustrated in Scheme 1. In physiological conditions, a partially unfolded or misfolded protein generally starts an aggregation process by nucleation-dependent oligomerization.[22] During the aggregation, oligomers (or the seeds) act as nucleation cores, and they gradually grow into intermediates and large protein aggregates (Scheme 1A).[22-24] However, this natural process usually takes a long time (i.e., several days, months, or more)[24-27] because the nucleation step is a rate-limiting step in protein aggregation.[22] Accordingly, if we add nanoparticles acting as nucleation cores to a free protein solution, as illustrated in Scheme 1B, the rate-limiting step can be omitted, and this accelerates the overall rate of protein aggregation. During the aggregation process, the nanoparticles act as nucleation cores and form networks depending on the structures of the protein aggregates (i.e., fibrillar aggregates or amorphous aggregates). Simultaneously, the nanoparticles assembled on the protein aggregates exhibit colorimetric responses in accordance with their interparticle distances and embedded shapes (i.e., longitudinal assembly and random clustering), as shown in Scheme 1B. For example, the deep blue color that is induced by the longitudinal assembly of nanoparticles implies the formation of fibrillar aggregates, and the violet color that is induced by the clustering of nanoparticles connotes the formation of amorphous aggregates. Consequently, we are able to rapidly detect the protein aggregates and predict in advance their morphological characteristics under destabilizing conditions with the naked eye (without instrumentation). For example, temperature, pH levels, chemicals, metal ions, and etc. can be factors for protein aggregation encountered in the physiological conditions.[28-33]

As a proof-of-concept demonstration, we examined acid-induced protein aggregation for small peptides of about 4 kDa [i.e., amyloid *β* (1-40) and amyloid *β* (1-42)] and a large protein of 32 kDa [i.e., superoxide dismutase 1 (SOD1)], which are implicated in Alzheimer's disease (AD) and amyotrophic lateral sclerosis, respectively. We describe our colorimetric detection concept that does not require instrumentation and validate it through conventional characterization tools. Finally we show that our proposed method can be utilized to screen the protein aggregation propensity under a variety of conditions such as high temperature, different pH levels, and chemicals.

Experimental

Materials

Amyloid *β* fragment 1-40 [A*β* (1-40)] and Amyloid *β* fragment 1-42 [A*β* (1-42)] were purchased from AnaSpec, Inc. (Fremont, CA, USA). SOD1 from human erythrocytes and all chemicals were purchased from Sigma-Aldrich Co. LLC (St. Louis, MO, USA). All water used in our experiment was purified to 18 MΩ.

Preparation of gold nanoparticles

The gold nanoplasmonic particles (GNPs, 17 nm in diameter) were prepared as described previously.[14] Briefly, the particles were prepared by boiling 100 mL of aqueous 0.01% (w/w) hydrogen tetrachloroaurate (III) trihydrate ($HAuCl_4 \cdot 3H_2O$) in a flask connected to a water-cooling column that was maintained at 98 °C with constant vigorous stirring and then adding 3 mL of 1% (w/w) sodium citrate ($Na_3C_6H_5O_7 \cdot 2H_2O$) all at once. When the color of the solution began to change, the heat was turned off, and the solution was allowed to cool to room temperature for about 20–30 min. The 520-nm

absorbance peak of the intrinsic 17-nm GNPs was observed with ultraviolet-visible (UV-Vis) spectroscopy, and its intensity was adjusted to 1.0 by dilution with deionized water for further experiments.

Spectral measurement with UV-Vis spectroscopy

In order to measure the spectral change induced by protein aggregation, 90 μL of GNPs was mixed with 10 μL of each protein solution at a physiologically relevant concentration range at the optimum ratio (9:1 v/v). To induce protein aggregation, we intentionally added 20 μL of hydrochloric acid (HCl) to the prepared mixture of the GNPs and each protein solution. Under the given acidic conditions, time-resolved spectra were collected with a UV-Vis spectrophotometer (DU 730, Beckman Coulter, Inc., Brea, CA, USA) and a precision cell (105.020-QS, 10 mm, Hellma GmbH & Co. KG, Müllheim, Germany).

Colorimetric assay with a microplate reader

The plasmon-based colorimetric assay for protein aggregation was performed with the samples, which were prepared by the same protocol described above for the spectral measurement method. In order to quantify the observed color change, the absorbance at a specific wavelength (i.e., 520 nm or 650 nm) for the mixture solution of each protein and the GNPs was measured with a SpectraMax M2e Microplate Reader (Molecular Devices LLC, Sunnyvale, CA, USA).

Dark-field microscopy

For the morphological analysis of the nanoparticle-assisted protein aggregation, an Olympus BX-43 (Olympus Corporation, Tokyo, Japan) microscope, equipped with an oil (or water) immersion dark-field condenser and CCD camera, was used. Each aliquot of the solutions was sampled onto a clean slide glass that had been pre-treated in a piranha solution (H_2SO_4:H_2O_2 = 7:3 v/v) for 1 h. A homemade polydimethylsiloxane fluidic chamber was prepared to confine the sample.

Circular dichroism (CD) spectroscopy

The secondary structures of each protein aggregate were characterized with a JASCO J-815 CD system (JASCO Inc., Easton, MD, USA). For typical far-UV protein spectra, a 1-mm rectangular quartz cuvette (110-QS, Hellma GmbH & Co. KG) was used, and the CD spectra were recorded from 190 nm to 250 nm. All of the CD measurements were conducted with the following parameters: 1 nm bandwidth, 100 nm/min run speed, 1 nm data pitch, and average of six runs.

Results and discussion

Spectral responses of concentration- and type-dependent protein aggregation

First, the two types of amyloid β (Aβ) peptides with different sequences, Aβ (1-40) and Aβ (1-42), which are abundant in patients with AD, were tested with our detection concept

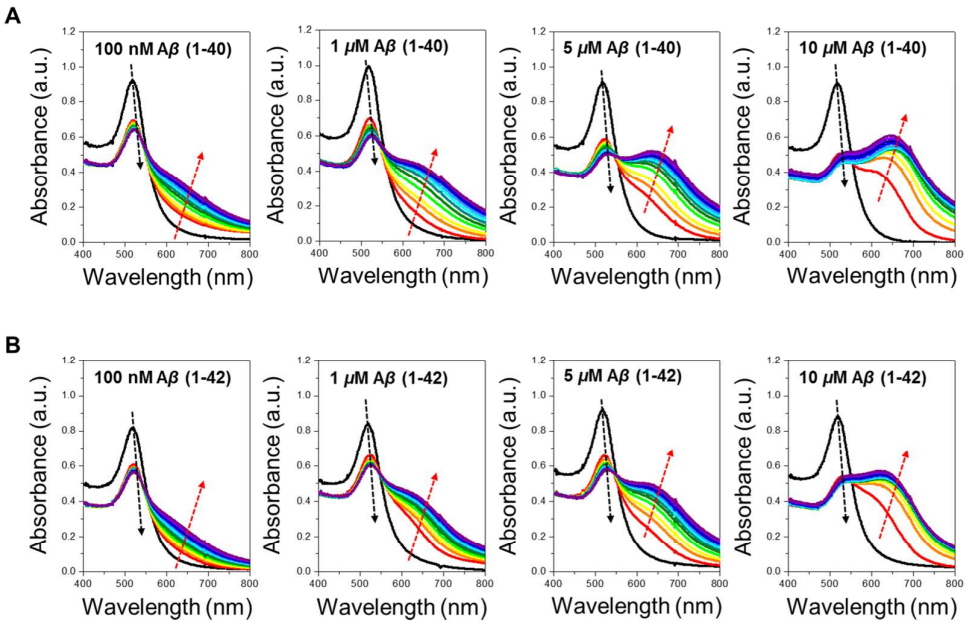

Fig. 1. Real-time monitoring of the Aβ concentration- and type-dependent aggregation with ultraviolet-visible (UV-Vis) spectroscopy. (A) Aβ (1-40) peptide. (B) Aβ (1-42) peptide. Real-time spectral changes in the mixture solution of Aβ peptides and gold nanoplasmonic particles (GNPs) were measured under acidic conditions. Various concentrations of the peptides were tested from 100 nM to 10 μM. The UV-Vis spectra were collected every 1 minute for 10 minutes. The arrows indicate the trends in the real-time spectral shift at the two absorbance bands of the intrinsic peak of GNPs (around 520 nm) and a newly formed larger aggregation indicator peak (around 650 nm).

described in Scheme 1. Synthesized GNPs (Optical Density: 1.0; ca, 1 nM) were mixed with Aβ (1-40) and Aβ (1-42) at physiologically relevant micromolar to nanomolar concentrations[27] so that the amounts of each peptide monomer were greater than the amounts of the GNPs. A small amount of 100 mM HCl was then added to the prepared mixture in order to induce protein aggregation under acidic conditions. The detailed experimental protocol is described in the Materials and Methods section. Low-pH conditions are well-known aggregation-promoting conditions, and these conditions have been extensively utilized to study protein aggregation.[24, 34-36]

Upon exposure to the acidic conditions, the time-resolved spectra of each mixture, including Aβ peptides and GNPs, were collected with UV-Vis spectroscopy (Fig. 1). For all of the cases, striking spectral changes were observed within a few minutes (see also Fig. S1 in ESI†). This dramatic change is probably due to rapid association between positively charged peptide (∵pI of Aβ≈pH 5.5)[17] and negatively charged GNP surface under acidic conditions, based on our control experiment under basic conditions (see also Fig. S2 in ESI†). For Aβ (1-40), as its concentration increased, the intensity of the intrinsic plasmon band of GNPs (around 520 nm) decreased, and another longer wavelength plasmon band (around 650 nm) appeared. The intensity increase around 650 nm was concentration-dependent. A longer plasmon band indicated the self-assembly of GNPs, which can be an indicator of the formation of larger Aβ aggregates (i.e., fibrillar aggregates and amorphous aggregates), as described in Scheme 1. The time-resolved spectra for Aβ (1-42) also showed concentration dependence. However, the rate of change in the spectra was relatively small compared to that for Aβ (1-40) (see also Fig. S1 in ESI†). It is consistent with previous reports presenting that Aβ peptides form fibrillar aggregates in acidic conditions (at pH ~2),[24, 35] and the fibrillization kinetics depends on the peptide sequences.[34, 37] Based on this, we can conclude that the observed spectral changes are very much related to the protein structure evolution, and the spectral differences depending on both the concentration and the type indicates a difference in the predominant protein structure during protein aggregation.

Colorimetric responses of concentration- and type-dependent protein aggregation

Having shown that the spectral changes are dependent on both the type and concentration of the peptides, we next examined the correlation of the collected spectra with the colors observed with the naked eye (Fig. 2A and 2B). We monitored the color change of the mixture solution over time. Significant and distinguishable color changes were observed within a few minutes (< 2 min), which was similar to the spectral changes observed with UV-Vis spectroscopy. Specifically, the Aβ (1-40) mixture solution showed a color transition from red to deep blue as the peptide concentration increased (Fig. 2A). Based on the spectral results (Fig. 1A), the deep blue color observed at the high concentration of over 10

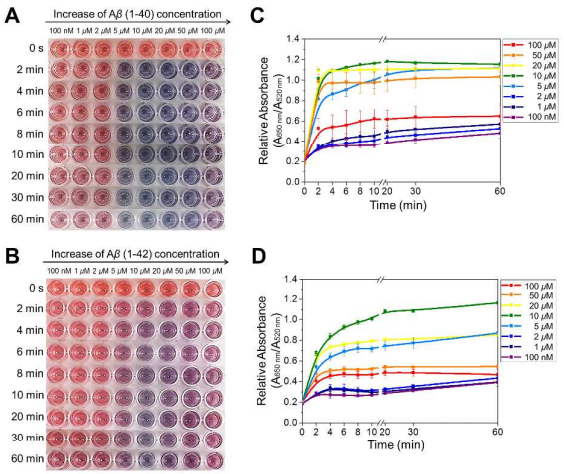

Fig. 2. Time-lapse colorimetric changes and kinetic profiles for the concentration- and type-dependent aggregation of Aβ. (A, B) The colorimetric responses of Aβ (1-40) aggregation (A) and Aβ (1-42) aggregation (B) measured from 100 nM to 100 μM for 60 min. (C, D) The concentration-dependent kinetic profiles for Aβ (1-40) aggregation (C) and Aβ (1-42) aggregation (D) described by the changes in relative absorbance ratios (A_{650nm}/A_{520nm}).

μM of the Aβ (1-40) peptide is related to the high intensity at the longitudinal plasmon band around 650 nm. Likewise, the violet color observed at the high concentration of Aβ (1-42) is related to the moderate intensity at 650 nm, which is comparable with the intensity at 520 nm (Fig. 1B and Fig. 2B).

In order to quantitatively analyze this colorimetric response, we also measured the spectral intensities at two absorbance peaks, the intrinsic peak of the GNPs (around 520 nm) and the newly formed larger aggregation indicator peak (around 650 nm), at each time frame with a conventional plate reader. Fig. 2C and 2D present plots for the intensity ratios between 520 nm and 650 nm showing the fast colorimetric response rate, which exhibit a steep slope following a saturation plateau and its clear concentration- and type-dependence. We also tested different sizes of GNPs. Results show that aggregation kinetics depends on the size of GNPs (see also Fig. S3 in ESI†) and 17-nm GNPs induce fast formation of the aggregation compared to smaller GNPs. And colorimetric responses for 17-nm GNPs are clearer compared to bigger GNPs. Based on our observation, there is no significant difference when we use GNPs of sizes around 15-20 nm. The reason why using 17-nm GNP is that it can be easily synthesized in the laboratory based on previously reported protocol.

Morphology analysis of nanoparticle-assisted protein aggregation

In order to determine if the observed colorimetric responses are related to the morphologies of the nanoparticle-assisted protein aggregates, the aggregates were examined with dark-field microscope imaging. Each aliquot of the reaction solutions was sampled onto a clean slide glass for morphology

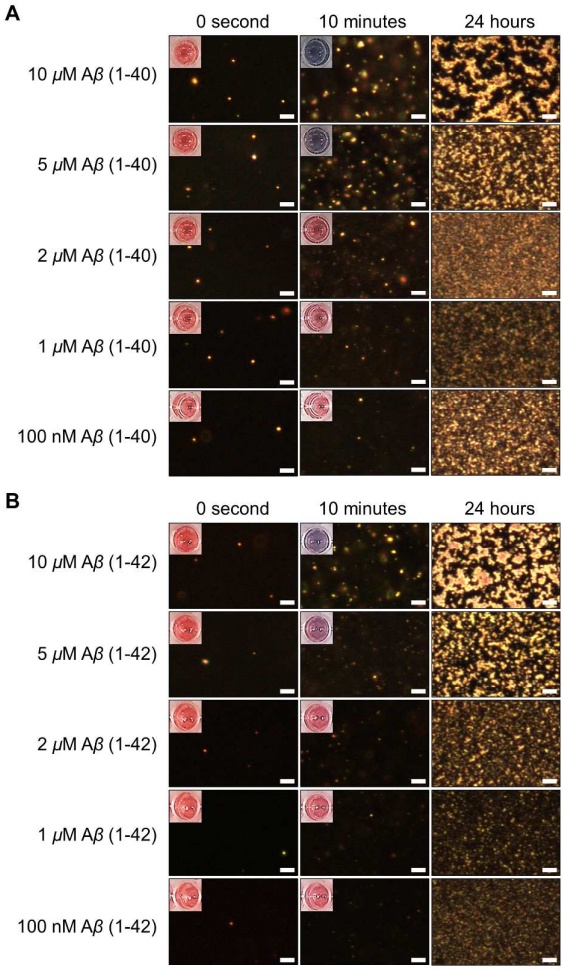

Fig. 3. Morphological analysis of the nanoparticle-assisted A*β* aggregation and its comparison with the colorimetric responses. (A, B) Dark-field images of the A*β* (1-40) peptides (A) and A*β* (1-42) peptides (B) incubated with nanoparticles under acidic conditions. Each inset shows a representative color of the sample solution. The images were taken from an initial point to 10 min and then 24 h later. Scale bars correspond to 20 μm.

analysis. Before exposure to the acidic conditions (0 second), the initial solution colors of all of the samples were red, and their corresponding dark-field images showed well-dispersed spots. Upon adding the HCl solution, the A*β* peptide concentration-dependent morphological evolution as well as color change was observed. After 10 min, the observed color transition to pink [e.g., 100 nM and 1 μM A*β* (1-40)], purple [e.g., 2 μM A*β* (1-40)], or deep blue [e.g., 5 μM and 10 μM A*β* (1-40)] was consistent with the increase in large aggregates, as shown in Fig. 3A. Because the color changes result from the distance-dependent light scattering of embedded GNPs in protein aggregates, we can correlate this color transition to pink, purple, or deep blue with the aggregation steps of small oligomeric assemblies, intermediate formation, or fibrillar aggregation, respectively. The concentration-dependent morphological evolution of protein aggregates, which was predictable from the earlier color change within a few minutes, was more clearly observed for the aggregates sampled after 24 h. At concentrations of A*β* (1-40) as high as 5 μM, fibril-like assembly was observed.

For A*β* (1-42), dark-field images showed a similar concentration-dependent morphological change as well as color change (pink, purple, or violet), while the deep blue color was not observed even at a higher concentration unlike with A*β* (1-40). These results are attributable to the difference in aggregation propensity depending on the peptide type.[31, 34, 36-38] In Fig. 3B, dark-field images of the aggregates formed after 24 h showed a trend of amorphous aggregation rather than fibrillar aggregation, which was consistent with the violet color (shown in insets) rather than deep blue. The morphological analysis suggests that the previously observed colorimetric responses can be utilized to predetermine the dominant structure evolution.

Characterization of secondary structures in the protein aggregates with CD spectra

In order to verify the structural evolution of the nanoparticle-assisted protein aggregation with that of physiological protein aggregation (without aid of nanoparticles), conventional CD spectra were collected for the A*β* (1-40) and A*β* (1-42) peptides incubated without GNPs under identical acidic conditions (Fig. 4). As incubation time increased, the CD spectra for A*β* (1-40) transitioned from a random coil (10 days) to *β* component-abundant (70 days) structures, which was obviously observed at a higher concentration (i.e., 10 μM) (Fig. 4A). We note that fibrillar aggregates are usually composed of *β* component-abundant structures.[39-42] Dark-field images showing the morphological evolution of small aggregates to large fibril-like aggregates (images on the left in Fig. 4A) were consistent with the observed changes (random coil to *β* component) in the protein secondary structures. It is noteworthy that our proposed method permits the predetermination of the propensity of protein aggregation, which usually takes a long time, with color in a very short time (shown in each inset).

Compared to A*β* (1-40), A*β* (1-42) underwent a slow transition to the *β* component under the same acidic conditions, which was also in good agreement with the nanoparticle-assisted A*β* aggregation results (Fig. 2C). The dark-field images of the large aggregates that were formed in 10 μM of the A*β* (1-42) mixture appeared relatively amorphous, which was consistent with the weaker signal in a CD spectrum (Fig. 4D) compared with the same concentration of A*β* (1-40). Taken together, these results emphasize that colorimetric responses reflect predominant protein structure evolution in certain destabilizing conditions.

Extended application to SOD1

In order to further confirm that our proposed method can apply to other proteins, SOD1, which is a dimeric protein of 32 kDa, was tested under a physiologically relevant concentration (~100 μM).[43,

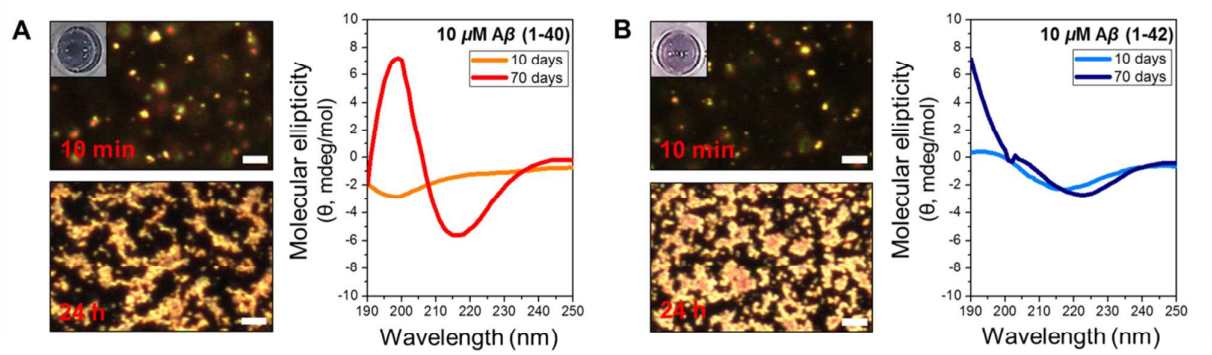

Fig. 4. Verification of the morphological evolution of nanoparticle-assisted protein aggregates with changes in the secondary structures of the protein aggregates that were formed without the aid of nanoparticles. (A) Dark-field images of the 10 μM Aβ (1-40) + GNP mixture solution after 10 min and 24 h exposure to the acidic conditions (left) and a colorimetric response of the solution after 10 min (inset). Circular dichroism (CD) spectra of 10 μM Aβ (1-40) incubated without GNPs under acidic conditions for 10 and 70 days (right). (B) Dark-field images of the 10 μM Aβ (1-42) + GNP mixture solution after 10 min and 24 h exposure to the acidic conditions (left) and a colorimetric response of the solution after 10 min (inset). CD spectra of 10 μM Aβ (1-42) incubated without GNPs under acidic conditions for 10 and 70 days (right). Scale bars correspond to 20 μm. Increases in the amounts of β-sheets were indicated by an increase of the negative band around 215 nm and the positive band around 195 nm.

[44] Under the identical experimental conditions, the results for the SOD1 protein showed a color transition to purple or violet (Fig. 5A). In addition, these colorimetric responses corresponded with the increase in the aggregates (from globular aggregates to amorphous aggregates) that were observed in the dark-field images (Fig. 5B). These results were in good agreement with the CD spectra showing a transition to a random coil-abundant structure rather than a β component-abundant structure. Our results correspond with previous reports that showed that SOD1 monomers tend to induce amorphous aggregates.[45-48]

Extended applications under a variety of conditions for protein aggregation

As mentioned before, there are many factors, which can affect protein aggregation encountered in the physiological conditions. For example, it is well-known that the factors such as temperature, pH levels, chemicals, metal ions, and etc. can induce protein aggregation without nanoparticles.[28-33] And these factors can also modulate the kinetics of the nanoparticle-promoted protein aggregation due to that conformational changes[28, 29, 32, 33, 49, 50] of proteins affect the association to the nanoparticles.[51-53] To confirm that our proposed method can be utilized to screen the protein aggregation propensity under a variety of conditions inducing protein aggregation, we additionally tested the nanoparticles-assisted protein aggregation under different destabilizing conditions such as high temperature, different pH levels, and chemicals (e.g., 2,2,2-Trifluoroethanol). Figure 6 shows representative plots for colorimetric responses implying the different kinetics of protein aggregation observed under different destabilizing conditions. Without nanoparticles, protein aggregation can occur in these destabilizing conditions and also undergoes the different kinetics. When we use nanoparticles as nucleators, the kinetics can be accelerated in most of cases. Kinetics of the nanoparticle-assisted protein aggregation is also dependent upon the destabilizing

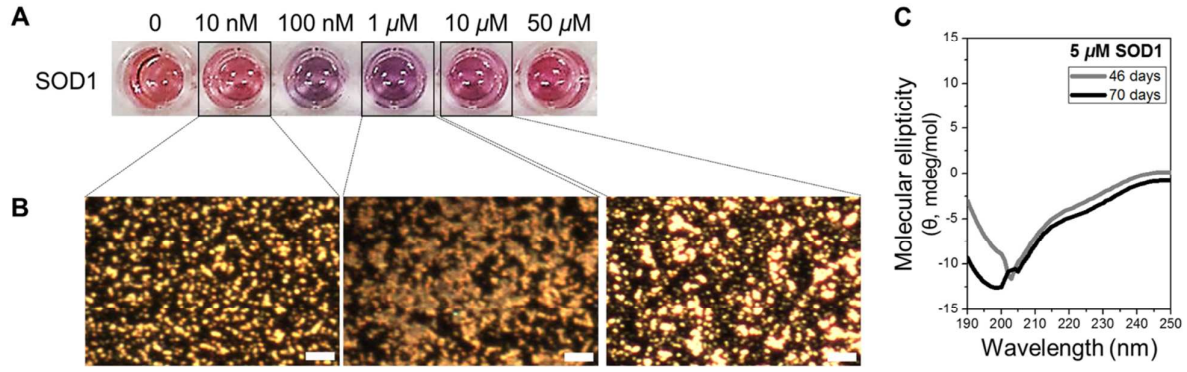

Fig. 5. Extended application results of the proposed method to another protein. (A) Concentration-dependent colorimetric responses for superoxide dismutase 1 (SOD1) aggregation. (B) Dark-field images of the nanoparticle-assisted SOD1 aggregates incubated under acidic conditions. Scale bars correspond to 20 μm. (C) CD spectra of 5 μM of SOD1 incubated without GNPs under identical acidic conditions for 46 and 70 days.

conditions, as such as protein aggregation without aids of nanoparticles depends on the exposed conditions. Based on our data (see also Fig. S4 and Fig. S5 in ESI†), kinetics of the nanoparticle-assisted protein aggregation under high temperature or strong acidic pH is much faster than protein aggregation under low temperature or weak acidic pH, as expected.

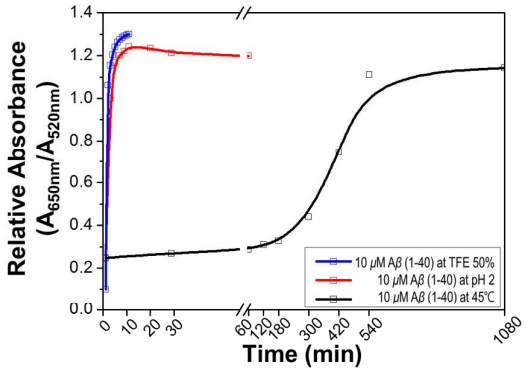

Fig. 6. Plots of colorimetric responses showing the different kinetics of protein aggregation observed under different destabilizing conditions (high temperature, acidic condition, and chemical denaturant).

Conclusion

In summary, we demonstrated a fast, simple, and easy method for studying protein aggregation with nanoparticle-assisted protein aggregation. We presented that our proposed method enabled us to predict protein aggregation propensities with the naked eye and without any instruments. As a demonstration of the concept, we monitored protein aggregation with A*β* (1-40) and A*β* (1-42) peptides in real-time and successfully predicted the predominant protein structures within a few minutes. Additionally, we showed the broad applicability of our concept by testing it with another protein (SOD1) and under various aggregation promoting conditions. We believe that our proposed method can be extended to studies of the molecular biophysics of protein aggregation and the rapid screening of anti-aggregation drugs for patients with protein conformational disease.

Acknowledgements

This work was supported by the 2014 Research Fund of the University of Seoul. This research was also supported by Basic Science Research Program through the National Research Foundation of Korea (NRF) funded by the Ministry of Science, ICT & Future Planning (2014R1A1A1038069).

Notes and references

1. R. W. Carrell and D. A. Lomas, *Lancet*, 1997, **350**, 134-138.
2. R. R. Kopito and D. Ron, *Nat. Cell. Biol.*, 2000, **2**, E207-209.
3. R. R. Kopito, *Trends Cell. Biol.*, 2000, **10**, 524-530.
4. M. Bartolini, C. Bertucci, M. L. Bolognesi, A. Cavalli, C. Melchiorre and V. Andrisano, *Chembiochem*, 2007, **8**, 2152-2161.
5. T. Ikeya, A. Sasaki, D. Sakakibara, Y. Shigemitsu, J. Hamatsu, T. Hanashima, M. Mishima, M. Yoshimasu, N. Hayashi, T. Mikawa, D. Nietlispach, M. Walchli, B. O. Smith, M. Shirakawa, P. Guntert and Y. Ito, *Nat. Protoc.*, 2010, **5**, 1051-1060.
6. F. Castellani, B. van Rossum, A. Diehl, M. Schubert, K. Rehbein and H. Oschkinat, *Nature*, 2002, **420**, 98-102.
7. B. Schuler, E. A. Lipman and W. A. Eaton, *Nature*, 2002, **419**, 743-747.
8. F. Schotte, M. H. Lim, T. A. Jackson, A. V. Smirnov, J. Soman, J. S. Olson, G. N. Phillips, M. Wulff and P. A. Anfinrud, *Science*, 2003, **300**, 1944-1947.
9. L. He, Y. Liu, J. Liu, Y. Xiong, J. Zheng, Y. Liu and Z. Tang, *Angew. Chem. Int. Ed.*, 2013, **52**, 3741-3745.
10. Z. Zhu, H. Meng, W. Liu, X. Liu, J. Gong, X. Qiu, L. Jiang, D. Wang and Z. Tang, *Angew. Chem. Int. Ed.*, 2011, **50**, 1593-1596.
11. S. Lee, H. D. Song, Y. I. Yang, G. P. Kim, I. Choi and J. Yi, *Chem. Commun.*, 2015, **51**, 213-216.
12. W. Liu, Z. Zhu, K. Deng, Z. Li, Y. Zhou, H. Qiu, Y. Gao, S. Che and Z. Tang, *J. Am. Chem. Soc.*, 2013, **135**, 9659-9664.
13. Z. Li, Z. Zhu, W. Liu, Y. Zhou, B. Han, Y. Gao and Z. Tang, *J. Am. Chem. Soc.*, 2012, **134**, 3322-3325.
14. S. Chah, M. R. Hammond and R. N. Zare, *Chem. Biol.*, 2005, **12**, 323-328.
15. S. Hong, I. Choi, S. Lee, Y. I. Yang, T. Kang and J. Yi, *Anal. Chem.*, 2009, **81**, 1378-1382.
16. I. Choi, Y. I. Yang, E. Jeong, K. Kim, S. Hong, T. Kang and J. Yi, *Chem. Commun.*, 2012, **48**, 2286-2288.
17. I. Choi and L. P. Lee, *ACS Nano*, 2013, **7**, 6268-6277.
18. J. Liu and Y. Lu, *Angew. Chem. Int. Ed.*, 2005, **45**, 90-94.
19. R. Elghanian, J. J. Storhoff, R. C. Mucic, R. L. Letsinger and C. A. Mirkin, *Science*, 1997, **277**, 1078-1081.
20. Y. Xia, T. D. Nguyen, M. Yang, B. Lee, A. Santos, P. Podsiadlo, Z. Tang, S. C. Glotzer and N. A. Kotov, *Nat. Nanotechnol.*, 2011, **6**, 580-587.
21. K. Kim, H. S. Han, I. Choi, C. Lee, S. Hong, S. H. Suh, L. P. Lee and T. Kang, *Nat. Commun.*, 2013, **4**, 2182.
22. J. C. Rochet and P. T. Lansbury, Jr., *Curr. Opin. Struct. Biol.*, 2000, **10**, 60-68.
23. C. M. Dobson, *Nature*, 2003, **426**, 884-890.
24. A. Lomakin, D. B. Teplow, D. A. Kirschner and G. B. Benedek, *Proc. Natl. Acad. Sci. USA*, 1997, **94**, 7942-7947.
25. M. E. M. Cromwell, E. Hilario and F. Jacobson, *AAPS. J.*, 2006, **8**, E572-E579.
26. S. Gao, H. C. Hendrie and K. S. Hall, *Arch. Gen. Psychiat.*, 1998, **55**, 809-815.
27. B. A. Yankner, L. K. Duffy and D. A. Kirschner, *Science*, 1990, **250**, 279-282.
28. M. S. Lin, L. Y. Chen, H. T. Tsai, S. S. S. Wang, Y. Chang, A. Higuchi and W. Y. Chen, *Langmuir*, 2008, **24**, 5802-5808.
29. T. H. J. Huang, D. S. Yang, N. P. Plaskos, S. Go, C. M. Yip, P. E. Fraser and A. Chakrabartty, *J. Mol. Biol.*, 2000, **297**, 73-87.
30. S. J. Wood, B. Maleeff, T. Hart and R. Wetzel, *J. Mol. Biol.*, 1996, **256**, 870-877.

31. C. J. Barrow, A. Yasuda, P. T. M. Kenny and M. G. Zagorski, *J. Mol. Biol.*, 1992, **225**, 1075-1093.
32. M. Bucciantini, E. Giannoni, F. Chiti, F. Baroni, L. Formigli, J. S. Zurdo, N. Taddei, G. Ramponi, C. M. Dobson and M. Stefani, *Nature*, 2002, **416**, 507-511.
33. A. M. Isaacs, D. B. Senn, M. L. Yuan, J. P. Shine and B. A. Yankner, *J. Biol. Chem.*, 2006, **281**, 27916-27923.
34. D. Burdick, B. Soreghan, M. Kwon, J. Kosmoski, M. Knauer, A. Henschen, J. Yates, C. Cotman and C. Glabe, *J. Biol. Chem.*, 1992, **267**, 546-554.
35. A. Lomakin, D. S. Chung, G. B. Benedek, D. A. Kirschner and D. B. Teplow, *Proc. Natl. Acad. Sci. USA*, 1996, **93**, 1125-1129.
36. W. B. Stine, Jr., K. N. Dahlgren, G. A. Krafft and M. J. LaDu, *J. Biol. Chem.*, 2003, **278**, 11612-11622.
37. P. E. Fraser, J. T. Nguyen, H. Inouye, W. K. Surewicz, D. J. Selkoe, M. B. Podlisny and D. A. Kirschner, *Biochemistry*, 1992, **31**, 10716-10723.
38. C. Hilbich, B. Kisterswoike, J. Reed, C. L. Masters and K. Beyreuther, *Eur. J. Biochem.*, 1991, **201**, 61-69.
39. H. Inouye, P. E. Fraser and D. A. Kirschner, *Biophysic. J.*, 1993, **64**, 502-519.
40. M. Sunde, L. C. Serpell, M. Bartlam, P. E. Fraser, M. B. Pepys and C. C. F. Blake, *J. Mol. Biol.*, 1997, **273**, 729-739.
41. S. B. Malinchik, H. Inouye, K. E. Szumowski and D. A. Kirschner, *Biophysic. J.*, 1998, **74**, 537-545.
42. C. Blake and L. Serpell, *Structure*, 1996, **4**, 989-998.
43. N. Kurobe, F. Suzuki, K. Okajima and K. Kato, *Clin. Chim. Acta*, 1990, **187**, 11-20.
44. J. Lindenau, H. Noack, H. Possel, K. Asayama and G. Wolf, *Glia*, 2000, **29**, 25-34.
45. C. A. Ross and M. A. Poirier, *Nat. Med.*, 2004, **10 Suppl**, S10-17.
46. A. Kerman, H. N. Liu, S. Croul, J. Bilbao, E. Rogaeva, L. Zinman, J. Robertson and A. Chakrabartty, *Acta Neuropathol.*, 2010, **119**, 335-344.
47. P. B. Stathopulos, J. A. O. Rumfeldt, G. A. Scholz, R. A. Irani, H. E. Frey, R. A. Hallewell, J. R. Lepock and E. M. Meiering, *Proc. Natl. Acad. Sci. USA*, 2003, **100**, 7021-7026.
48. I. Choi, Y. I. Yang, H. D. Song, J. S. Lee, T. Kang, J. J. Sung and J. Yi, *Biochim. Biophys. Acta-Mol. Basis Dis.*, 2011, **1812**, 41-48.
49. K. Ma, E. L. Clancy, Y. B. Zhang, D. G. Ray, K. Wollenberg and M. G. Zagorski, *J. Am. Chem. Soc.*, 1999, **121**, 8698-8706.
50. M. Bartolini, C. Bertucci, V. Cavrini and V. Andrisano, *Biochem. Pharmacol.*, 2003, **65**, 407-416.
51. S. Linse, C. Cabaleiro-Lago, W. F. Xue, I. Lynch, S. Lindman, E. Thulin, S. E. Radford and K. A. Dawson, *Proc. Natl. Acad. Sci. USA*, 2007, **104**, 8691-8696.
52. Y. Hoshino, H. Lee and Y. Miura, *Polym. J.*, 2014, **46**, 537-545.
53. M. Zheng, Z. G. Li and X. Y. Huang, *Langmuir*, 2004, **20**, 4226-4235.